X-RAY/UV OBSERVING CAMPAIGN ON THE MRK 279 AGN OUTFLOW: A GLOBAL FITTING ANALYSIS OF THE UV ABSORPTION [1]

Jack R. Gabel[2], Nahum Arav[2], Jelle S. Kaastra[3], Gerard A. Kriss[4,5], Ehud Behar[6], Elisa Costantini[3,7], C. Martin Gaskell[8], Kirk T. Korista[9], Ari Laor[6], Frits Paerels[10], Daniel Proga[11], Jessica Kim Quijano[4], Masao Sako[12], Jennifer E. Scott[4], Katrien C. Steenbrugge[3]

Accepted for publication in ApJ

ABSTRACT

We present an analysis of the intrinsic UV absorption in the Seyfert 1 galaxy Mrk 279 based on simultaneous long observations with the *Hubble Space Telescope* (41 ks) and the *Far Ultraviolet Spectroscopic Explorer* (91 ks). To extract the line-of-sight covering factors and ionic column densities, we separately fit two groups of absorption lines: the Lyman series and the CNO lithium-like doublets. For the CNO doublets we assume that all three ions share the same covering factors. The fitting method applied here overcomes some limitations of the traditional method using individual doublet pairs; it allows for the treatment of more complex, physically realistic scenarios for the absorption-emission geometry and eliminates systematic errors that we show are introduced by spectral noise. We derive velocity-dependent solutions based on two models of geometrical covering – a single covering factor for all background emission sources, and separate covering factors for the continuum and emission lines. Although both models give good statistical fits to the observed absorption, we favor the model with two covering factors because: (a) the best-fit covering factors for both emission sources are similar for the independent Lyman series and CNO doublet fits; (b) the fits are consistent with full coverage of the continuum source and partial coverage of the emission lines by the absorbers, as expected from the relative sizes of the nuclear emission components; and (c) it provides a natural explanation for variability in the Lyα absorption detected in an earlier epoch. We also explore physical and geometrical constraints on the outflow from these results.

Subject headings: galaxies: individual (Mrk 279) — galaxies: active — galaxies: Seyfert — ultraviolet: galaxies

1. INTRODUCTION

Mass outflow, seen as blueshifted absorption in UV and X-ray spectra, is an important component of active galactic nuclei (AGNs; see recent review in Crenshaw, Kraemer, & George 2003). This "intrinsic

[1] Based on observations made with the NASA/ESA *Hubble Space Telescope* and the NASA-CNES-CSA *Far Ultraviolet Spectroscopic Explorer*, and obtained at the Space Telescope Science Institute, which is operated by the Association of Universities for Research in Astronomy, Inc. under NASA contract NAS 5-26555.
[2] Center for Astrophysics and Space Astronomy, University of Colorado, 389 UCB, Boulder CO 80309-0389; jgabel@colorado.edu, arav@colorado.edu
[3] SRON National Institute for Space Research, Sorbonnelaan 2, 3584 CA Utrecht, The Netherlands; J.S.Kaastra@sron.nl, e.costantini.sron.nl, K.C.Steenbrugge@sron.nl
[4] Space Telescope Science Institute, 3700 San Martin Drive, Baltimore, MD 21218; gak@stsci.edu; jescott@stsci.edu; jkim@stsci.edu
[5] Center for Astrophysical Sciences, Department of Physics and Astronomy, The Johns Hopkins University, Baltimore, MD 21218
[6] Department of Physics, Technion, Haifa 32000, Israel; behar@physics.technion.ac.il, laor@physics.technion.ac.il
[7] Astronomical Institute, University of Utrecht, PO Box 80 000, 3508 TA Utrecht, The Netherlands
[8] Department of Physics and Astronomy, University of Nebraska, Lincoln NE 68588-0111; mgaskell1@unl.edu
[9] Department of Physics, Western Michigan University, Kalamazoo, MI 49008; korista@wmich.edu
[10] Columbia Astrophysics Laboratory, 550 West 120th Street, New York, NY 10027; frits@astro.columbia.edu
[11] JILA, University of Colorado, Campus Box 440, Boulder, CO 80309; proga@colorado.edu
[12] Theoretical Astrophysics and Space Radiation Laboratory, California Institute of Technology, MC 130-33, Pasadena, CA 91125; masao@tapir.caltech.edu

absorption" is ubiquitous in nearby AGNs, appearing in over half of Seyfert 1 galaxies having high-quality UV spectra obtained with the *Hubble Space Telescope* (*HST*; Crenshaw et al. 1999) and the *Far Ultraviolet Spectroscopic Explorer* (*FUSE*; Kriss 2002). Spectra from the *Advanced Satellite for Cosmology and Astrophysics (ASCA)* identified X-ray "warm absorbers", seen as absorption edges, in a similar percentage of objects (Reynolds 1997; George et al. 1998). Large total ejected masses have been inferred for these outflows, exceeding the accretion rate of the central black hole in some cases, indicating mass outflow plays an important role in the overall energetics in AGNs (e.g. Reynolds 1997). Recent studies have recognized and explored the potential effect of outflows on all scales of the AGN environment, from feeding the central supermassive black hole in AGNs (Blandford & Begelman 1999, 2004), to influencing the evolution of the host galaxy (Silk & Rees 1998; Scannapieco & Oh 2004) and the metallicity of the intergalactic medium (Cavaliere, Lapi, & Menci 2002).

Measured ionic column densities provide the basis for interpretation of the physical nature of AGN outflows. Detailed UV spectral studies over the past decade have shown measurements of these crucial parameters are often not straightforward. Analyses of absorption doublets and multiplets has revealed the absorbers typically only partially occult the background emission sources. Without proper treatment of this effect, the column densities could be severely in error (e.g. Wampler, Bergeron, & Petitjean 1993; Barlow & Sargent 1997; Hamann et al. 1997). Addi-

tional complications that could affect column density measurements are different covering factors for different background emission sources (Ganguly et al. 1999; Gabel et al. 2003), velocity-dependent covering factors (e.g. Arav et al. 1999), and inhomogeneous distributions of absorbing material (de Kool, Korista, & Arav 2002).

Many recent investigations of AGN outflows have focused on intensive multiwavelength observations of Seyfert 1 galaxies. Seyferts are well suited for these studies because they include the brightest AGNs in the UV and X-ray. The X-ray spectra contain the imprint of the bulk of the outflow's mass, which can now be deblended into individual absorption lines with the high-resolution capabilities of the *Chandra X-ray Observatory (CXO)* and *XMM-Newton Space Observatory*, allowing detailed study. The high quality UV spectra available with *HST* and *FUSE* provide a complimentary, precise probe of the complex absorption troughs. Due to the relatively narrow absorption in Seyfert outflows, the important UV doublets and multiplets are typically unblended, allowing measurements of these key diagnostic lines.

We have undertaken an intensive multiwavelength observing campaign with *HST*/STIS, *FUSE*, and *CXO* to study the intrinsic absorption in the Seyfert 1 galaxy Mrk 279. Mrk 279 was selected for this study because of its UV and X-ray brightness and the rich absorption spectrum in both bands, including unblended and well-resolved UV doublets (see Scott et al. 2004, hereafter SK04). Additionally, it has minimal contamination by Galactic absorption and a relatively weak contribution from a narrow emission line region (NLR), both of which can complicate measurements of the absorption properties. As part of a series of papers devoted to this campaign, we present here a detailed study of the UV absorption in the combined STIS and *FUSE* spectra. We develop a new approach for measuring the covering factors and column densities in the absorbers, making full use of the high quality far-UV spectrum. These measurements provide the foundation for subsequent analysis and interpretation of the mass outflow in Mrk 279, and provide novel geometric constraints. In parallel papers, we present analysis of the X-ray spectrum (Costantini et al. 2004), inhomogeneous models of the UV absorption (Arav et al. 2004), and density diagnostics based on O v K-shell X-ray lines (Kaastra et al. 2004). In future papers, we will present photoionization models of the UV and X-ray absorption and analysis of absorption variability. In the next section, we describe the *HST* and *FUSE* observations and present an overview of the absorption spectrum; in §3, we review the standard doublet technique for measuring intrinsic absorption and, together with an Appendix, discuss important limitations of this method; the formalism of our fitting method and results for Mrk 279 are described in §4; in §5, the fits are interpreted, and implications for physical constraints on the outflow are explored; finally, a summary is presented in §6.

2. OBSERVATIONS AND THE INTRINSIC ABSORPTION SPECTRUM

2.1. *Simultaneous HST/STIS and FUSE Observations of Mrk 279*

The nucleus of Mrk 279 was observed for a total of 41 ks (16 orbits) with the Space Telescope Imaging Spectro-

graph (STIS) on board *HST* between 2003 May 13 – 18 and for 91 ks with *FUSE* between 2003 May 12 – 14. The STIS observation used the E140M grating, which covers 1150 – 1730 Å, and was obtained through the $0''.2 \times 0''.2$ aperture. The spectrum was processed with CALSTIS v2.16, which removes the background light from each echelle order using the scattered light model from Lindler & Bowers (2000). Low residual fluxes in the cores of saturated Galactic lines indicate accurate removal of scattered light: typical fluxes in the cores are $\pm < 2.5\%$ of the local unabsorbed continuum flux levels, and mean fluxes averaged over the absorption cores are $< 3\%$ of the noise in the troughs. The final spectrum was sampled in $0.012 – 0.017$ Å bins, thereby preserving the ~ 6.5 km s^{-1} kinematic resolution of STIS/E140M.

We found that the standard pipeline processing did not yield a fully calibrated spectrum due to two effects: a) the echelle ripple structure, due to the characteristic efficiency of the detector along each order, is not completely removed (see Heap & Brown 1997), and b) the sensitivity of the MAMA detectors has degraded with time, and the change has not been incorporated in the pipeline for the echelle gratings. In order to correct for these effects in the Mrk 279 spectrum, we used multiple spectra of the white dwarf spectrophotometric standard, BD+28 4122, one of which was taken close in time to our observation. First, a composite stellar spectrum of BD+28 4122 composed of FOS and STIS data (Bohlin, Kickinson, & Calzetti 2001) was used to flux-calibrate a 1997 STIS spectrum of BD+28 4122 that does not exhibit the echelle ripple structure. This flux-calibrated spectrum was then used to correct a STIS spectrum of BD+28 4122, taken on 3 May 2003 with the same grating and aperture as our Mrk 279 observation, and which does show the same ripple structure seen in the Mrk 279 spectrum. These two corrections were performed by dividing the fiducial spectrum for each step by the comparison spectrum, fitting a polynomial to the result, and then multiplying the comparison spectrum by that polynomial. We used the polynomials from the second step described above to correct the spectrum of Mrk 279. To obtain a smooth correction for each order in the Mrk 279 spectrum, we applied averages of the polynomials corresponding to the four adjacent orders. Although we were able to remove most of the echelle ripple structure in this way, some lower amplitude residual curvature remains in some orders. However, the intrinsic absorption features measured in this study are well-corrected.

The *FUSE* spectrum, obtained through the $30'' \times 30''$ aperture, covers 905 – 1187 Å. The spectrum was processed with the current standard calibration pipeline, CALFUSE v2.2.3. The eight individual spectra obtained with *FUSE*, from the combination of four mirror/grating channels and two detectors, were coadded for all exposures. Mean residual fluxes measured in the cores of saturated Galactic lines are consistent with zero within the noise (i.e., standard deviation of the fluxes) in the troughs of these lines, indicating accurate background removal. The spectrum was resampled into $\sim 0.02 – 0.03$ Å bins to increase the signal-to-noise ratio (S/N) and preserve the full resolution of *FUSE*, which is nominally ~ 20 km s^{-1}.

To place the *FUSE* and STIS spectra on the proper

TABLE 1
KINEMATICS OF ABSORPTION
COMPONENTS IN MRK 279[a]

Component	Velocity [b] km s^{-1}	FWHM km s^{-1}
1	85	40
2	-265	50
2a	-290	30
2b	-325	30
2c	-355	65
3	-390	20
4	-460	20
4a	-490	65
5	-550	30

[a]Measurements for components 2, 2a, 2c, and 4a are from the N V λ1242 line; components 1, 2b, 3, 4, and 5 are from Si III and C III.

[b]Radial velocity relative to the systemic redshift adopted for Mrk 279, z =0.305

wavelength scale, we followed the procedure described in SK04. The centroids of prominent, unblended Galactic interstellar absorption lines were measured and used as fiducials in comparing to the Galactic 21 cm H I line in the line-of-sight to Mrk 279 (Wakker et al. 2001). The lines measured in the STIS spectrum are consistent with the 21 cm H I line within the measurement uncertainties and thus required no correction. The *FUSE* spectrum showed substantial shifts relative to the adopted standard. Due to non-linear offsets in the wavelength scale, local shifts were measured and applied individually to each spectral region containing intrinsic absorption features.

To normalize the absorption, we fit the total intrinsic (i.e., unabsorbed) AGN emission in the *FUSE* and STIS spectra over each intrinsic absorption feature. This was done empirically by fitting cubic splines to unabsorbed spectral regions adjacent to the features, at intervals of ~ 5 Å . We also derived models for the individual contributions of the different emission sources (continuum and emission lines), since they are required for our analysis. For the continuum source, we fit a single power law ($f_\lambda \propto \lambda^{-\alpha}$) to the observed flux at two widely separated wavelengths that are relatively uncontaminated with absorption or line emission features, λ = 955 and 1500 Å. After first correcting for Galactic extinction (using the extinction law of Cardelli, Clayton, & Mathis 1989, with $E(B-V) = 0.016$), we find a best-fit spectral index $\alpha = 1.6$. This power law model matches the few other line-free regions of the UV spectrum, i.e. $\lambda \approx 1150$ – 1180, 1330, and 1390 Å, to within a few percent. Thus, for the emission line model, we simply subtracted the continuum power law model from the empirical fit to the total emission.

2.2. *The Far-UV Absorption Spectrum*

The full far-UV spectrum from our *FUSE* and STIS observations is shown in Figure 1. The active nucleus in Mrk 279 was in a relatively high flux state during this epoch; the UV continuum flux was similar to a 2000 January *FUSE* observation, and ≈ 7 times stronger

than in *FUSE* and STIS spectra obtained in 2002 May. Full treatment of these earlier observations is given in SK04. Qualitatively, the intrinsic absorption spectrum in our new observations is similar to the earlier epochs (although some important variations were detected that will be the subject of a later study). Here, we give a brief overview, and refer the reader to SK04 for a more thorough phenomenological discussion of the absorption.

Absorption from a range of ions is detected around the systemic velocity of the host galaxy, between $v = -600$ to $+150$ km s^{-1}; we adopt the redshift for Mrk 279 from SK04, $z = 0.0305 \pm 0.0003$. Normalized absorption profiles for some of the prominent lines are shown in Figure 2. The absorption is seen to be resolved into multiple distinct kinematic components at the resolution of STIS E140M and *FUSE*, revealing striking differences in the kinematic structure of different ions. Low-ionization species appear in several narrow components (see Si III in Figure 2, but also Si II, C II, C III, and N III in SK04 Figures 7 – 14). However, the more highly ionized O VI, N V, and C IV doublets, which are the primary UV signatures of intrinsic absorption in AGNs, are much broader and have different centroid velocities. The Lyman lines exhibit the kinematic structure of the low-ionization components, but also appear in the lower outflow velocity region coinciding with the high-ionization lines, $v \approx -300$ to -200 km s^{-1}.

We adopt the component numbering system from SK04, which was based on the kinematic structure in Lyβ. In Figure 2, dotted vertical lines mark the centroids of the components in SK04 that exhibit narrow absorption structure in low-ionization species in the current spectrum but which have no corresponding structure in the high-ionization CNO doublets. Centroids of the components seen in the high-ionization lines are identified with dashed lines; we have added component 2c to the SK04 system based on structure in the C IV and N V profiles. Measured centroid radial velocities and widths of the components are listed in Table 1. The differences in ionization and kinematic structure between these two
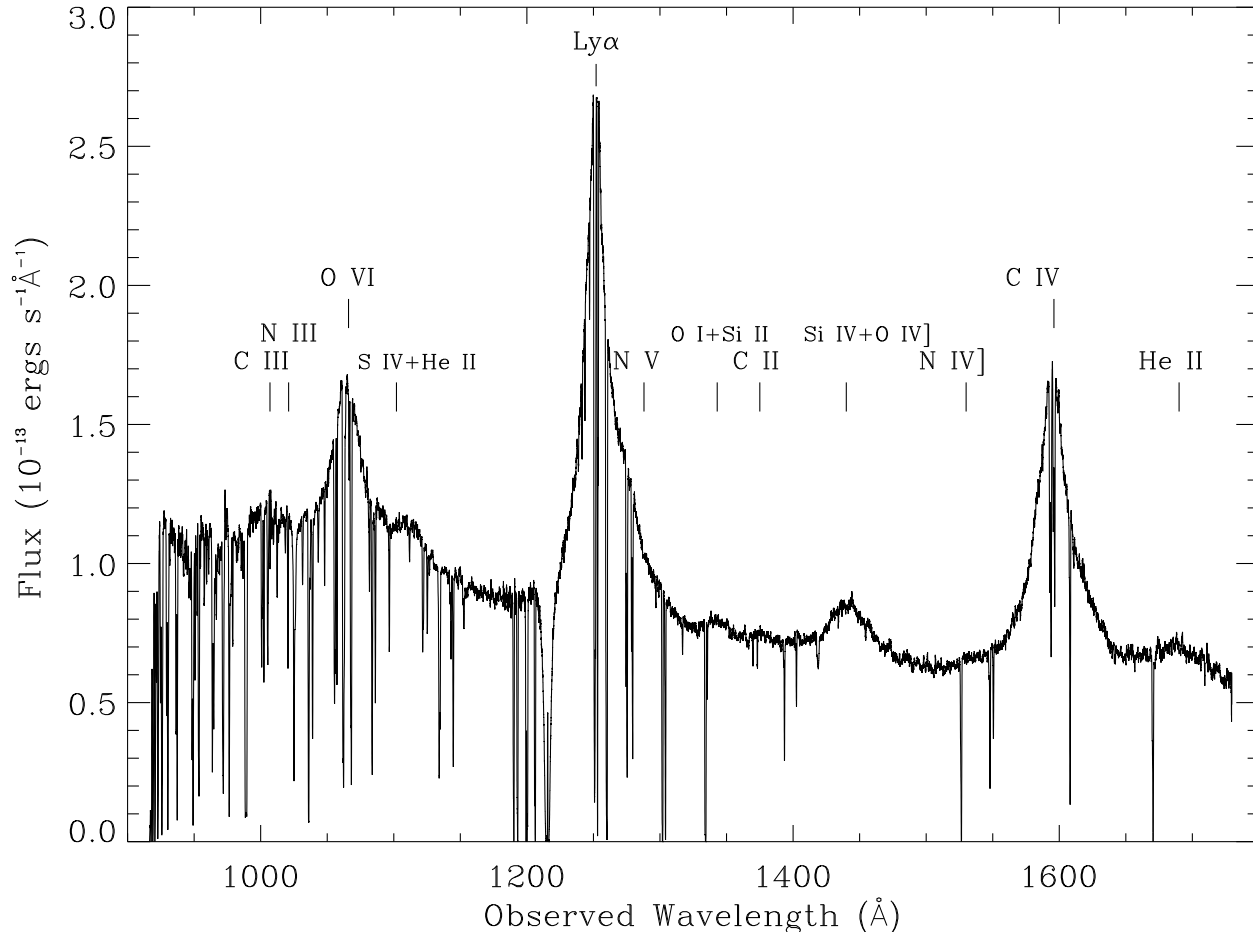
FIG. 1.— Full far-UV spectrum of the active nucleus in Mrk 279 from the *FUSE* and *HST*/STIS spectra obtained in May 2003. Emission lines are labeled above the spectrum. The data were heavily binned for clarity in presentation.

groups of components strongly suggests they are physically distinct. Based on their ionization, narrow widths, distinct centroid velocities, and (in component 4) low density implied by the stringent upper limit on the C II column density in the excited fine-structure level, SK04 concluded at least some of the low-ionization components are not associated with the AGN outflow. Instead, they posited they are associated with gas located at relatively large distances from the nucleus - perhaps from an interaction with the companion galaxy MCG+12-13-024, high-velocity clouds associated with the host galaxy of Mrk 279, or, in the case of component 1, in the interstellar medium of the host galaxy.

In this study, we restrict our attention to the *bona fide* intrinsic absorption, i.e., that presumed to be directly associated with an outflow from the AGN. We take this to include all absorption from the broad O VI, N V, and C IV doublets; Figure 2 shows that any absorption associated with the narrow low-ionization components will at most only effect the outer wings of the outflow components in these lines. Conversely, Figure 2 shows Lyman line absorption from the low-ionization components is strong and heavily blended with the intrinsic absorption components; thus, we limit our analysis of H I to the uncontaminated region, $v \approx -300$ to -200 km s^{-1}.

3. THE DOUBLET METHOD: OVERVIEW AND LIMITATIONS

We present here a brief review of the standard technique for measuring UV absorption in AGN outflows and describe some limitations of this method to highlight the motivation for our method of analysis. In earlier studies of intrinsic absorption, the red members of doublet pairs were often found to be deeper than expected relative to the blue lines, based on their intrinsic 2:1 optical depth ratios. In many cases this was interpreted as due to partial coverage of the background nuclear emission by the absorbing gas, e.g., Wampler, Bergeron, & Petitjean (1993), Barlow & Sargent (1997), Hamann et al. (1997); (other possibilities are scattering from an extended region and emission from an extended source unrelated to the central engine of the AGN; Cohen et al. 1995; Goodrich & Miller 1995; Kraemer et al. 2001). If partial coverage is not accounted for, the absorption ionic column densities can be severely underestimated, which will dramatically affect the interpretation of the outflow. The expression for the observed absorption that includes the effects of line-of-sight covering factor (C) and optical depth (τ) is:

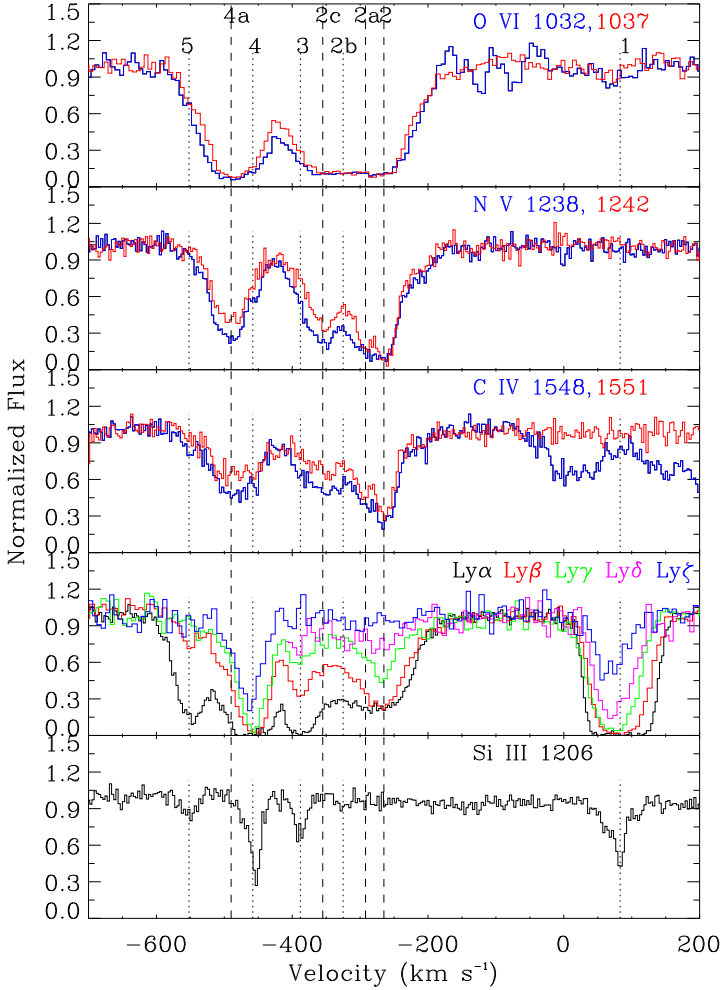$$I(v) = (1 - C(v)) + C(v)e^{-\tau(v)}, \qquad (1)$$

FIG. 2.— Normalized absorption profiles from 2003 May STIS and *FUSE* spectra. The spectra are plotted as a function of radial velocity with respect to the systemic redshift of the host galaxy. The centroid velocities of kinematic components associated with the AGN outflow are identified with dashed vertical lines. Components identifying low-ionization absorbers likely unrelated to the outflow (see text) are shown with dotted lines. The difference in kinematic structure is evident in comparing the high-ionization CNO doublets with Si III. The Lyδ profile is not plotted at $v < -400$ km s^{-1} due to contamination with Galactic absorption at these velocities.

where I is the normalized flux, and all quantities are written as a function of radial velocity, v. Since the optical depths of the UV doublet pairs are in the simple 2:1 ratio, equation 1 can be solved for the covering factor and optical depths of each doublet (Barlow & Sargent 1997; Hamann et al. 1997). The resulting expressions, which we will refer to as the doublet solution, are:

$$C = \frac{I_r^2 - 2I_r + 1}{I_b - 2I_r + 1}, \qquad (2)$$

$$\tau_r = -\ln(\frac{I_r - I_b}{1 - I_r}), \qquad (3)$$

where r and b subscripts identify the red and blue members of the doublet, and the equation for τ was derived by Arav, Korista, & de Kool (2002). These expressions can be evaluated for unblended (i.e., sufficiently narrow) absorption doublets with members that are individually resolved, and derived as a function of radial velocity.

While this has provided a revolutionary advance in the study of intrinsic AGN absorption, there are some key limitations to this method, described below.

3.1. *Multi-Component Nature of the Background Emission*

An implicit assumption in the doublet solution is that the absorption is imprinted on a uniform, homogeneous background emission source, since it allows for the solution of only a single C and τ. However, the AGN emission is comprised of multiple, physically distinct sources, i.e., a continuum source and emission line regions (including multiple kinematic components), which have different sizes, morphologies, and flux distributions. Thus, in cases where the absorber only partially occults the total background emission, the distinct sources would be expected to have different line-of-sight covering factors, in general. This possibility was first explored by Ganguly et al. (1999) for the continuum source and broad emission line region (BLR), and was demonstrated in the intrinsic absorption systems by Ganguly et al., Gabel et al. (2003), Hall et al. (2003), and SK04.

To account for multiple discrete background emission sources, equation 1 can be expanded to give the normalized flux of the jth line

$$I_j = \Sigma_i[R_j^i(C_j^i e^{-\tau_j} + 1 - C_j^i)], \qquad (4)$$

where the ith individual emission source contributes a fraction $R_j^i = F_j^i/\Sigma_i[F_j^i]$ to the total intrinsic flux and has covering factor C_j^i. The *effective* covering factor for each line is the weighted combination of individual covering factors, and can be written:

$$C_j = \Sigma_i C_j^i R_j^i \qquad (5)$$

These are expansions of the expressions given in Ganguly et al. (1999) to include an arbitrary number of emission sources.

The multi-component nature of the background emission has several important implications for the analysis of AGN outflows:

• From equation 5 it can be seen that lines of the same ion could have different effective covering factors, which may introduce an error into the doublet equation. This happens when the underlying emission fluxes differ from the spectral position of one line to the other and is illustrated in the N V doublet absorption shown in Figure 3. Here, the emission line flux underlying the blue member is ≈ 15% greater than under the red line, while the continuum flux under the two lines is identical. The magnitude of this error depends on the slopes of the flux distributions between the doublet lines and differences in individual covering factors of the distinct emission sources. Ganguly et al. (1999) showed this effect is typically small when considering the continuum/BLR distinction, due to the gradual slope of the BLR; however, if the doublet lines are near saturation, it could have a very large effect since small flux differences correspond to large optical depth differences in these cases. Also, an underlying narrow emission line component could have a pronounced effect on the solution (Arav, Korista, & de Kool 2002; Kraemer et al. 2002; Gabel, Kraemer, & Crenshaw 2004).

• Without separation of the covering factors of the distinct sources, covering factors derived from a doublet pair
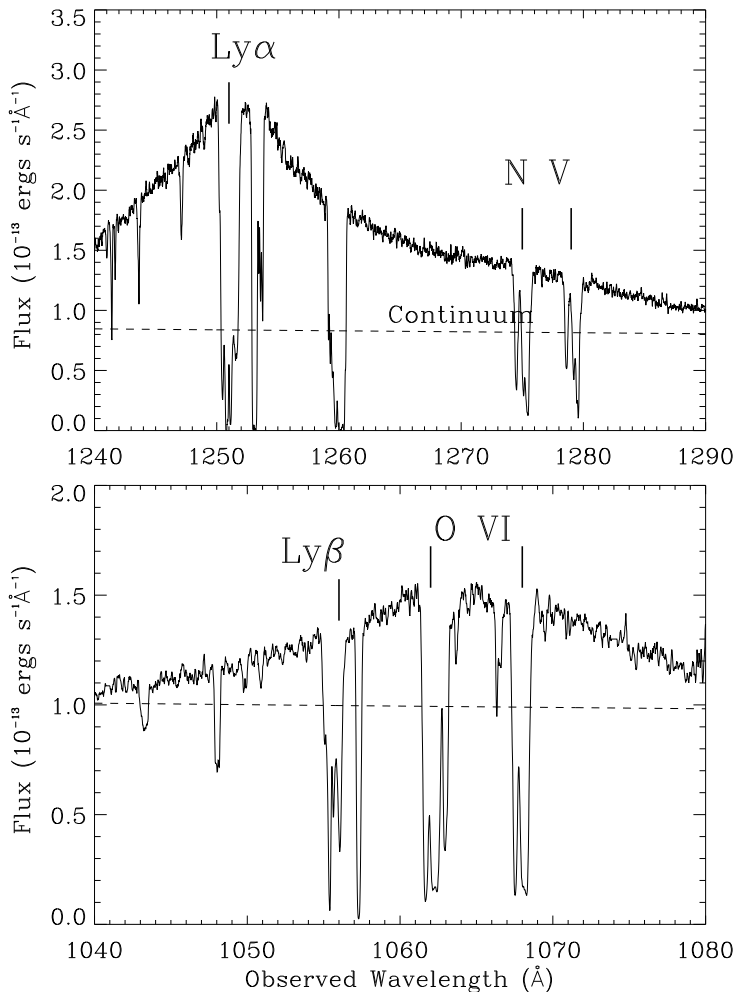
FIG. 3.— Spectrum of Lyα - N V (top panel) and Lyβ - O VI (bottom panel), illustrating complexities in treating covering factors in intrinsic absorption measurements. The continuum flux level, plotted as dashed lines, is essentially identical for each pair of lines, while the emission-line fluxes underlying each line differs greatly. This has important implications for the relative *effective* covering factors. Additionally, the nature of the BLR emission underlying these lines is complex: Lyβ absorption lies on the high-velocity blue wing of O VI, while N V absorption has a contribution from the red wing of the Lyα BLR.

cannot be applied to measure column densities of other lines. This is evident in Figure 3; clearly the effective covering factor derived for N V is not applicable to Lyα if the individual continuum and emission-line covering factors differ since Lyα has much more underlying line flux. Similarly, Lyβ, plotted in the bottom panel in Figure 3, will not generally have the same effective covering factor as Lyα, due to the different emission line contributions under each line. However, if the individual covering factors are known, effective covering factors can be constructed for any line using equation 5. This is important for measuring singlet lines or contaminated multiplets that have no independent measure of the covering factor.

• Finally, the doublet solution misses potentially important, unique constraints on the absorption and emission geometry. For example, combined with estimates of the sizes of the individual sources derived from other techniques, the individual covering factors constrain the size of the absorber, e.g. Gabel et al. (2003), and the rel-

ative location of the different emission components and absorber as projected on the plane of the sky. The individual covering factors can also serve as a unique probe of more detailed geometry of the background emission. Consider for example the O VI – Lyβ spectrum shown in Figure 3. The O VI doublet absorbs its own emission line flux at the blueshifted velocity of the outflow ($v_{BLR} \approx -600$ to -200 km s^{-1}), while the Lyβ absorber sits primarily on the high-velocity blue wing of the O VI BLR at $v_{BLR} \approx -2200$ km s^{-1}. The Lyβ line emission is relatively weak. Similarly, there is a contribution from the extreme red wing of the Lyα BLR profile under the N V absorption. Constraints on the emission line covering factors for these lines could be used to probe the kinematic-geometric structure of the BLR; the absorber can thus serve as a filter to view and explore the background AGN sources.

3.2. *Systematic Errors in the C – τ Solutions*

Another limitation is that the doublet method always gives a solution, but it is often difficult to gauge its accuracy due to the non-linear dependency of the solution on measurement errors. To explore this, we have generated synthetic absorption profiles that include random fluctuations simulating spectral noise, and calculated C and τ using the doublet equations. Illustrative results are shown in an Appendix, whereas a complete quantitative treatment will be presented in a later paper. We find there are systematic errors in the solutions that can give misleading results. These errors are not random about the actual value, but rather systematically underestimate the actual covering factor, as seen in the Appendix; the discrepancy in the solution increases with weaker absorption doublets and decreased S/N. Additionally, Ganguly et al. (1999) demonstrated that the finite instrumental line spread function can lead to further systematic errors in the doublet solution.

4. OPTIMIZATION FITTING OF THE INTRINSIC ABSORPTION: LYMAN SERIES AND CNO DOUBLET GLOBAL LINE FITS

Motivated by the limitations of the traditional doublet method described above, we introduce here a different approach for measuring intrinsic absorption. The underlying principle is to increase the number of lines that are simultaneously fit in order to (a) explore additional parameters contributing to the formation of observed absorption troughs and (b) overconstrain the set of equations. This allows for the treatment of more complex, physically realistic scenarios of the absorption-emission geometry. By minimizing errors to simultaneous fits of multiple lines, noise in the spectrum will generally be smoothed out, in contrast to the erratic behavior of the doublet solution demonstrated in §3.2 and the Appendix.

4.1. *Formalism*

Our fitting algorithm employs the Levenberg-Marquardt non-linear least-squares minimization technique to solve equation 4 for specified absorption parameters (C_j^i, τ_j)[13]. It is similar in principle to

that used in SK04 to analyze the Lyman lines in earlier spectra of Mrk 279. Given a total of n observed absorption lines (I_j) as constraints, up to n−1 parameters can be modeled. No a priori assumptions are made about the kinematic distribution of the covering factors and optical depths of the absorbing material (e.g., Gaussian) – indeed, one goal is to solve for the velocity-dependent absorption parameters to constrain the kinematic-geometric structure of the mass outflow. Thus, we derive fits to the absorption equations for each velocity bin. This also avoids errors in the solutions resulting from averaging over variable profiles. The algorithm minimizes the χ^2 function, with each data point appropriately weighted by the 1 σ errors, which are a combination of spectral noise and estimated uncertainties in fitting the intrinsic underlying fluxes. For the latter, the continuum flux uncertainties were determined from the residuals between the power-law model and the line-free regions of the spectrum. We estimated uncertainties in the emission-line fluxes by testing different empirical fits over the absorption features, finding the range that gave what we deemed reasonable line profile shapes.

The key requirement in employing this technique is to link multiple absorption lines for simultaneous fitting. There are two general ways to do this:

• *Lines from the Same Energy Level:* The most straightforward way is to fit all available lines arising from the same ionic energy level, thereby eliminating uncertainties in ionic abundances or level populations. If the relative underlying fluxes from distinct emission sources differs between the lines, the individual covering factors of those emission sources can be derived. In the subsequent analysis, we fit all of the uncontaminated Lyman series lines in Mrk 279. These lines are ideal because they span a very large range in optical depth and have significantly different amounts of underlying emission-line flux (see Gabel et al. 2003). Additionally, the full set of lines is accessible in low redshift AGNs with combined *FUSE* and STIS spectra. We note the Fe II UV multiplets, which appear in a small fraction of AGN absorbers (de Kool et al. 2001; Kraemer et al. 2001), are another promising set of lines for this analysis.

• *Global Fitting Approach:* The second approach involves linking lines from different ions (or any group of lines arising from different levels) by placing physically motivated constraints on their absorption parameters. In our analysis of Mrk 279 below, we fit the six combined lines of the O VI, N V, and C IV doublets by assuming they share the same covering factors. Another potential application of this method is to link the absorption for a given line in spectra from different epochs via assumptions about the relative values of the absorption parameters between epochs (e.g., assuming the covering factors did not change). The validity of the assumptions used to link the equations can then be tested by the result of the fit.

4.2. *Covering Factor and Optical Depth Solutions for Mrk 279*

For the intrinsic absorption in Mrk 279, we independently fit the two groups of lines described above: the Lyman series lines and the combined CNO doublets, i.e. global fit. For each set of lines, we tested two differ-

ent models of the absorption covering factor. In model A, a single covering factor was assumed to describe all lines, i.e., no distinction was made between the different emission sources. In model B, independent covering factors for the continuum source and emission lines, C^c and C^l, were assumed. In this case, the general expressions in equations 4 and 5 reduce to those in Ganguly et al. (1999).

For the Lyman lines, the solvable range is limited to $-300 \lesssim v \lesssim -200$ km s^{-1}, due to blending with the narrow, low-ionization components in the high velocity region of the outflow (see §2.2). This is due to the failure of equation 4 where multiple absorption components with different covering factors contribute in the same velocity bin; there is no straightforward way to disentangle how the different absorbers overlap as projected against the background emission sources. Figure 2 shows Lyα, Lyβ, and Lyγ give the best constraints for the Lyman series analysis, exhibiting clean well-defined absorption profiles at relatively high S/N. Weak absorption in Lyδ is also present in component 2, while Lyϵ is contaminated with Galactic H$_2$ absorption and thus omitted from the fitting. Lyζ is not detected in components 2 – 2a within the limits of the spectral noise, thus to reduce the effect of noise on the solution, we set the normalized flux to unity for this line. All lines of higher order than Lyζ were omitted from the analysis since they exhibit no intrinsic absorption and provide no additional constraints. Thus, there are five lines as constraints to fit the two and three free parameters for the Lyman solution in model A and B, respectively.

For the global fitting of the O VI, N V, and C IV doublets, the absorption equations were linked by assuming their covering factors are equal (separately for the continuum and emission lines in model B). The optical depth of each ion is a free parameter. As described in §2.2 and seen in Figure 2, these lines are not strongly contaminated by the narrow, low-ionization absorption that dominates the Lyman lines; at most, there is only weak contamination in the wings of the broad, intrinsic absorption features by these low-ionization systems.

Best-fits to the covering factors and optical depths (or equivalently column densities) for both line groups are shown in Figure 4 (model A) and Figure 5 (model B). In all cases, the parameter space search for the covering factors was restricted to the physically meaningful range, $0 \leq C^i \leq 1$. The plotted error bars represent the formal 1 σ statistical errors in the best-fit parameters. Specifically, these correspond to values giving $\Delta\chi^2 =1$, and were computed from the diagonal elements of the covariance matrix for the optimal fit (Bevington 1969). For cases where the covering factor solution is a boundary value (0,1), e.g. much of the C^c solution for the CNO doublets in model B, no covariance matrix elements are computed for that parameter since it is not a minimum in the solution. For these cases, we estimated uncertainties by deriving solutions for models keeping the parameter fixed, and finding the value giving $\Delta\chi^2 =1$ from the best-fit solution at the boundary value. To ensure the computations did not erroneously stop at local minima, we generated solutions using different starting points for the parameter search space; identical results were found in all cases. The fitted profiles, derived by inserting the best-fit solutions into equation 4, for both models (model
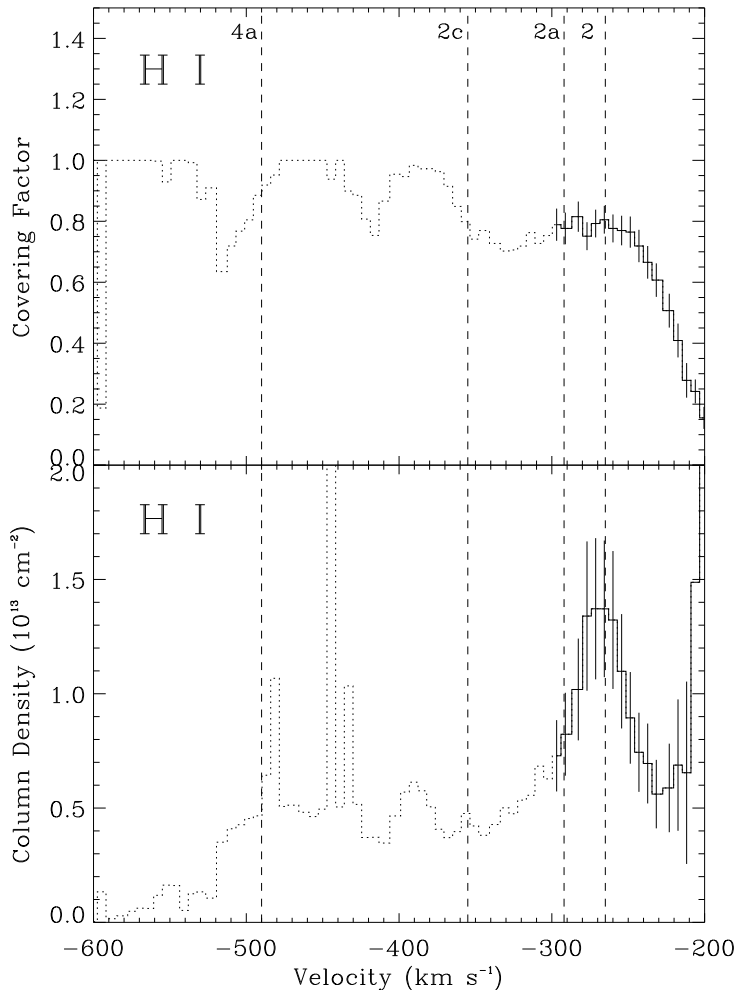
Fig. 4.— Best-fit covering factor and column density/optical depth solutions from χ^2 minimization for the single covering factor geometric model (model A). Top panels show C solutions, solved independently for the Lyman series (left panels) and combined CNO doublets (right). Bottom panels show the H I column density and C IV (dashed histogram), N V (dotted), and O VI (solid) optical depth solutions. The contaminated, and thus unreliable, region of H I absorption is plotted with dotted histograms.

A in blue, model B in red) are compared with the observed normalized absorption profiles in Figure 6.

4.3. *Errors and Uncertainties*

There are some possible errors in this fitting that should be mentioned. First, the emission lines are treated as all arising from a single component. Line emission from distinct kinematic components, i.e. broad, intermediate, narrow line regions, that are covered by different fractions by the absorbers could introduce an error into the solution (although, the narrow line region in Mrk 279 is relatively weak). Also, there are cases where absorption features sit on the BLR emission from different lines and thus sample different velocities of the BLR profile (i.e., Lyβ and N V described in §3.1 and shown in Figure 3). This could introduce an error into the solution if there are spatial inhomogeneities in the BLR gas as a function of velocity. Second, the area on the sky sampled by the *FUSE* aperture is four orders of magnitude greater than the STIS aperture. While this has no consequences for
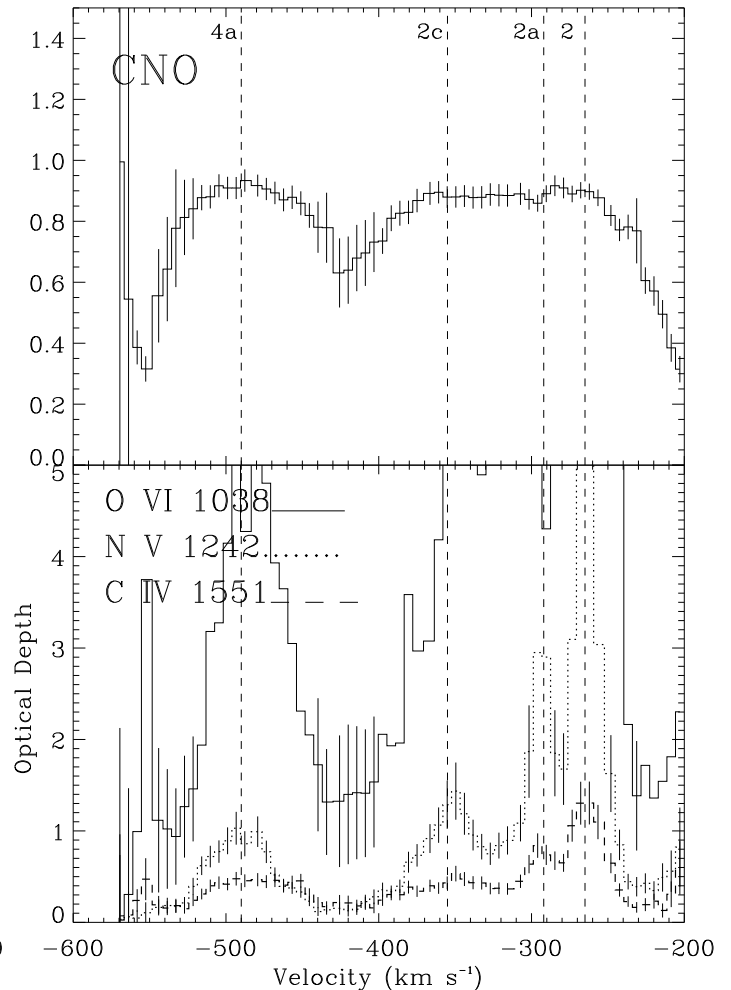
the continuum and BLR emission, which are unresolved and much smaller than the 0.″2 STIS aperture, any extended emission might effect the solutions. This could include scattering of nuclear emission by an extended scatterer (e.g. Kraemer et al. 2001) or extended O VI NLR emission. Finally, we have assumed the absorption optical depth of each line (τ_j) is uniform across the lateral extent of the emission sources, and thus the absorber is completely homogeneous (see de Kool, Korista, & Arav 2002). Models departing from this assumption are presented in Arav et al. (2004).

5. DISCUSSION AND INTERPRETATION

5.1. *Favored Absorption Model: Independent Continuum and Emission Line Covering Factors*

Figure 6 shows both geometric models are able to match the intrinsic absorption features well at most outflow velocities, indicating the solutions for these models and parameters are degenerate over much of the profiles. There are some regions fit somewhat better by model B, particularly C IV in the low-velocity outflow component. However, there is additional, stronger evidence that supports the two covering factor model for the outflow, as outlined below.

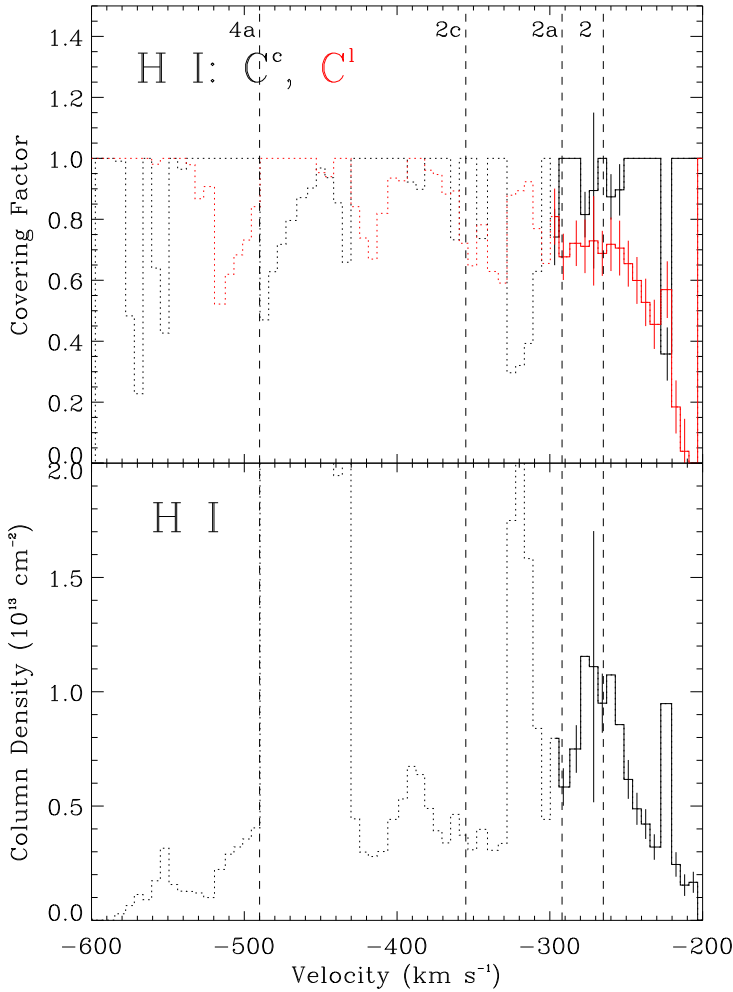• *Consistent Covering Factor Solutions From the In-*

FIG. 5.— Same as Figure 4 for the two covering factor geometric model (model B). Continuum covering factors are plotted in black and emission-line covering factors in red.
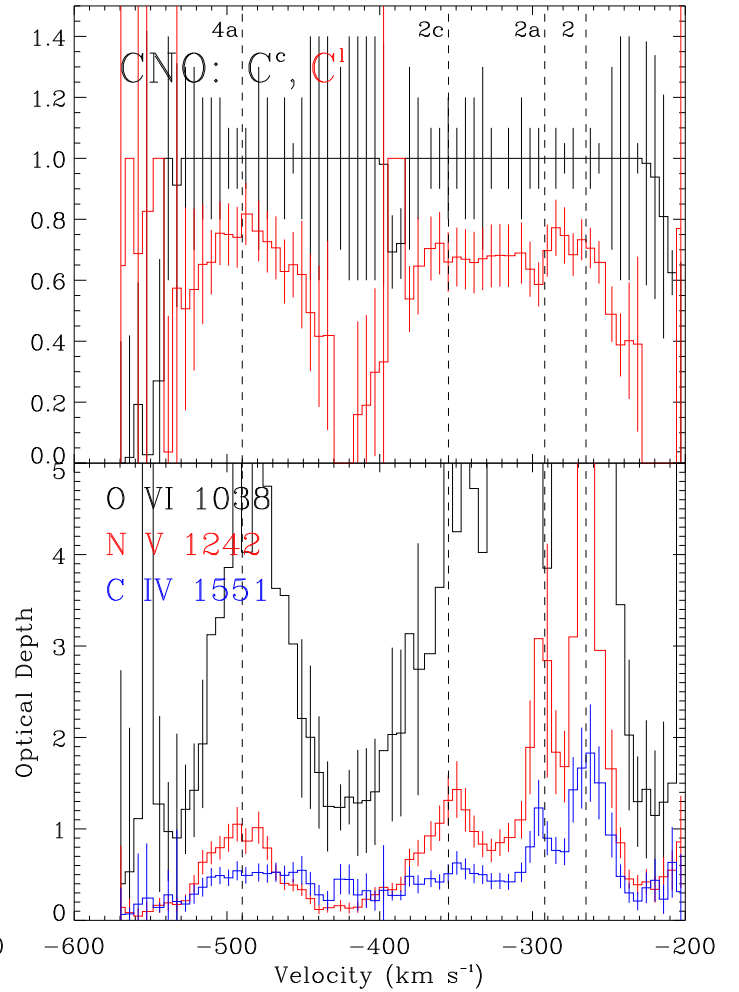
FIG. 5.—

dependent Lyman Line and Global CNO Doublet Fitting Methods: Figure 5 shows that both the Lyman and global CNO doublet best-fit solutions are consistent with full coverage of the continuum source over most of the velocity range with a valid Lyman solution. Further, the independent solutions for the two groups of lines are plotted together in Figure 7 for a direct comparison; the emission line covering factor profiles computed in model B are shown in the top panel and the single covering factors derived in model A are in the bottom panel. The H I and CNO C^l fits are nearly identical over most of the core region of the absorption, with $C^l \approx 0.7$ (although in the wing of the absorption, $v > -250$ km s^{-1}, the solutions diverge somewhat). In contrast, the Lyman method solution in model A is systematically less than the global doublet solution by about $0.1 - 0.15$ at all velocities.

• *Consistency with the Emission Source Sizes:* The continuum and emission line covering factor solutions in model B are also physically consistent with our understanding of the sizes of those emission sources. Reverberation mapping studies of AGNs have shown the BLR is substantially larger than the ionizing continuum source. These studies measure the BLR to be several to tens of light-days across (e.g. Peterson et al. 1998; Kaspi et al.

2000), while the UV continuum source is likely at least an order of magnitude smaller in size and possibly much smaller (e.g. Laor & Netzer 1989; Proga 2003). Thus, the solution of a fully covered continuum source and partial coverage of the emission lines is consistent with the nuclear emission geometry. The fact that this result was arrived at separately with the independent Lyman and global CNO fits is compelling.

• *Variability in Lyα Absorption:* In Figure 8, the normalized Lyα profile from our observation is compared with the STIS spectrum obtained a year earlier, showing the absorption was shallower in the previous epoch by ∼ 0.15 in normalized flux units. This variability is not due to a lower H I column density; the strength of Lyβ in a contemporaneous *FUSE* observation indicates Lyα was saturated in the earlier epoch (SK04), as it is in the 2003 spectrum, hence the profiles in both epochs simply delineate the unoccluted flux. Thus, a change in covering factor must be responsible for the observed variability. Noting that the emission line-to-continuum flux ratio was greater in the 2002 spectrum than in 2003, we tested if the difference in covering factor of the respective sources could explain the variability. To this end, we constructed a synthetic absorption profile for Lyα in the 2002 epoch based on the results from our analysis of the 2003 spec-
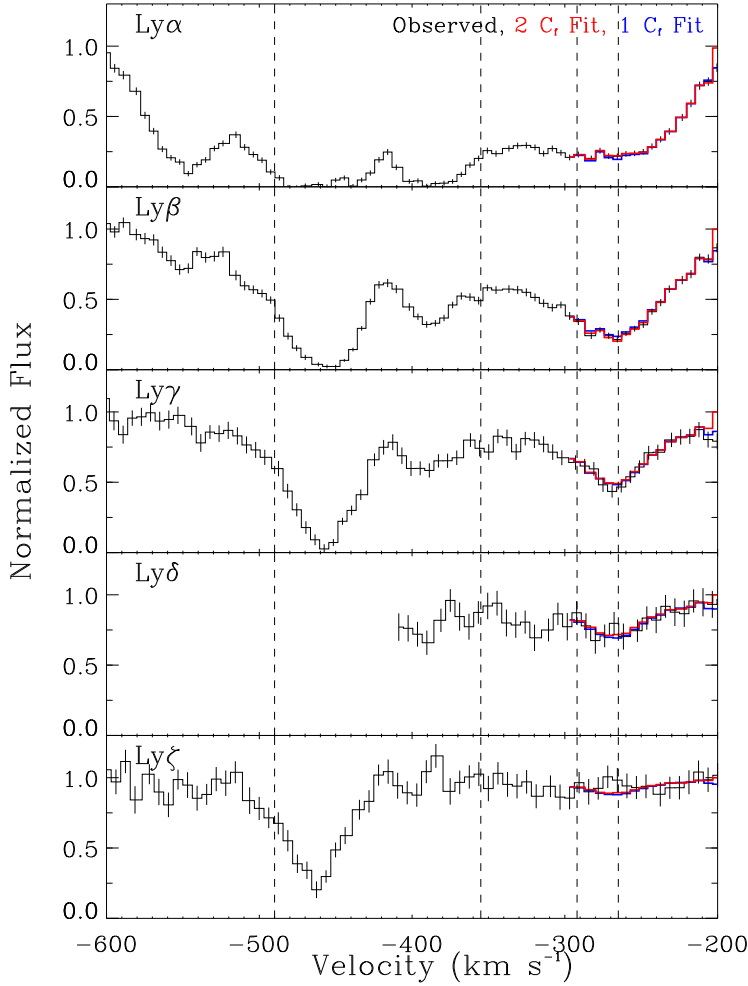
FIG. 6.— Best-fit intrinsic absorption profiles for the Lyman lines (left) and CNO doublets (right) from the two geometric models. The normalized observed spectrum is plotted in black, model A profiles are in blue, and model B profiles in red. The model profiles were derived from the best-fit covering factors and column densities shown in Figures 3 and 4 using equation 4. The contaminated region of the Lyman line fit (dotted lines in Figures 3,4) is not plotted.

FIG. 6.—

trum. Specifically, we set $C^c = 1$ at all velocities, and solved for C^l in the 2003 Lyα profile. The observed continuum and emission line fluxes in the 2002 spectrum were then weighted by these covering factors according to equation 4. The resulting model profile, shown in the bottom panel of Figure 8, matches the observed absorption very well. This provides a natural explanation for the variability in the Lyα absorption profile: the covering factors of each source individually remain the same, but a change in the *effective* covering factor occurs due to different relative strengths of the distinct background emission components.

5.2. *Comparison of Solutions from Different Methods*

The covering factor and optical depth solutions for C IV, N V, and O VI from the two-C global fit (model B) are compared with the single doublet solutions (equations 2 and 3) in Figure 9. The global fit effective covering factors are weighted combinations of the individual covering factors shown in Figure 5, derived using equa-
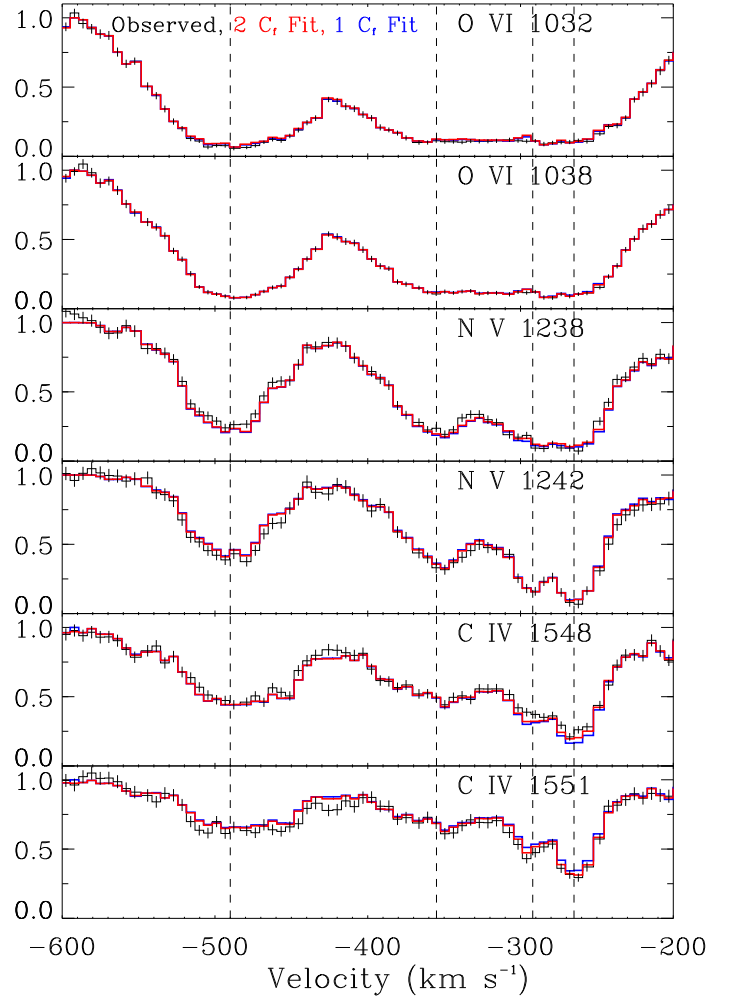
tion 5. In Figure 9, solid red lines show C profiles for the short-wavelength members of each doublet and dotted lines show results for the long-wavelength lines; they are nearly identical in all cases, indicating negligible errors in the doublet solution due to different contributions from underlying line emission (see first bullet in §3.1).

Figure 9 shows the solutions from the two methods differ significantly in some regions, with important implications for the kinematic-geometric and -ionization structure in the outflow. For example, the doublet covering factor solution, plotted in black, exhibits much more velocity-dependence than the global fit. This is seen, for example, in the wings of C IV and N V in component 4a and the red wing of component 2, where C decreases strongly in the wings, while the optical depth profiles show little or no relation to the absorption trough structure when compared with Figure 2. Further, the kinematic structure in these ions is much different from the O VI solution. In these cases, the doublet solution implies the observed absorption profiles are determined almost entirely by velocity-dependent covering factor. Additionally, in some regions, particularly in C IV, the doublet solutions for C and τ exhibit sharp fluctuations over small velocity intervals that do not coincide with structure in the observed absorption features, nor with the solutions
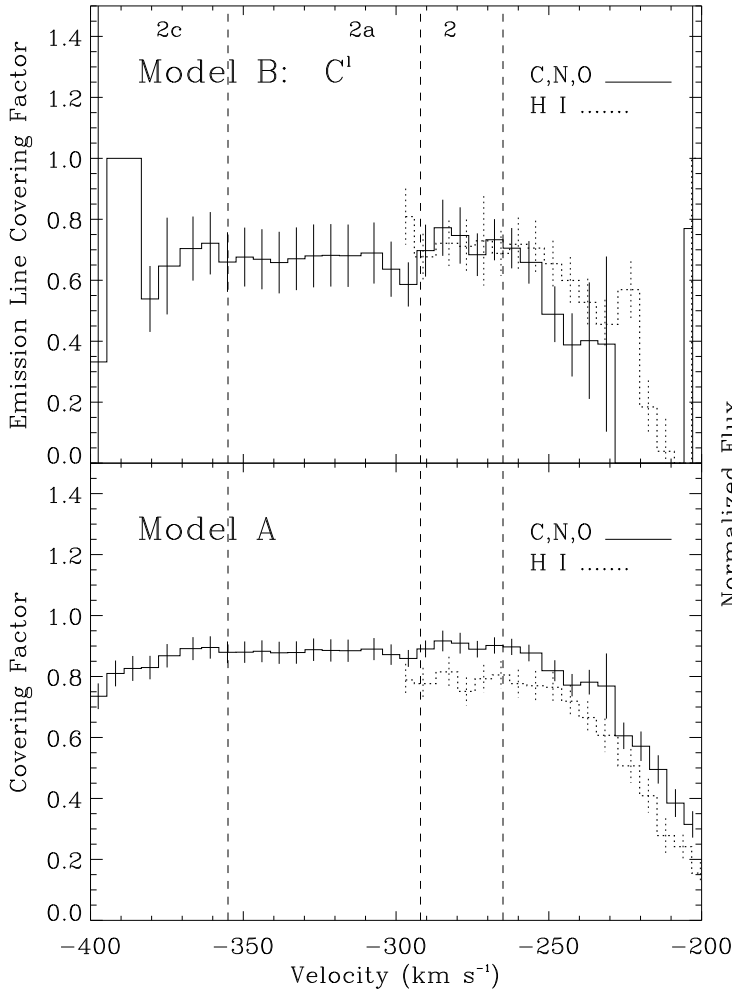
FIG. 7.— Comparison of covering factor solutions for the two independent methods – Lyman and global CNO doublet lines. Best-fit solutions to the emission-line covering factors from model B are shown in the top panel. The single covering factor solutions from model A are in the bottom panel.

FIG. 8.— Variability in Lyα absorption. The top panel shows Lyα absorption in components 2–2a was shallower in a May 2002 STIS spectrum (solid histogram) than in May 2003 (dashed). The bottom panel shows a model of the 2002 profile (dotted), constructed with individual covering factors derived from the 2003 spectrum (Figure 5), matches the observed profile well. This indicates the variation in absorption depth is likely due to a change in *effective* covering factor resulting from different relative strengths of the continuum and emission-line fluxes in the two epochs.

from the other ions (e.g., components 2a – 2c, and 4a).

Comparison with the observed profiles in Figure 2 shows these effects in the doublet solution are strongly correlated with the absorption strength. Smaller derived covering factors are associated with weaker absorption, both in the wings of individual kinematic components and in overall absorption features, such as C IV components 2c and 2a. As discussed in the Appendix and §3.2, synthetic absorption profiles show the doublet solution suffers from systematic errors consistent with this general trend – spectral noise causes an underestimate of the covering factor. The simulations we present in the Appendix indicate the solutions become unreliable for cases where $\tau \lesssim 1$ in the blue doublet member, and increasingly so for lower τ. This, combined with the large, seemingly random fluctuations seen in certain regions suggests some features in the doublet solutions in Figure 9 are artifacts due to noise and not real features in the outflow. However, one puzzling aspect of the solutions, in comparison to the results in the Appendix, is that there are not more negative values for the covering factors. The simulations predict that for sufficiently low optical depth, there is a high probability that $C < 0$. This should be especially
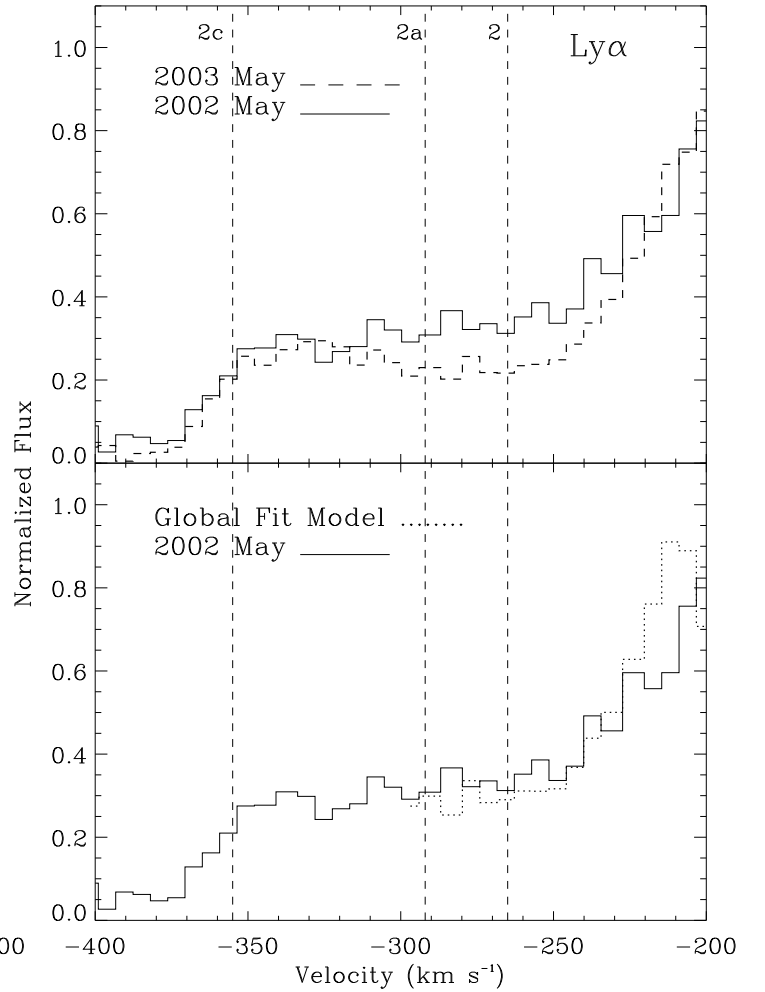
apparent for intermediate values of τ, such as the middle two models presented in the Appendix, where dramatic fluctuations between large positive and negative values are expected. It is unclear why this is not more prevalent in the solutions in Figure 9.

In Table 2, we compare integrated column densities measured from the different solutions: the two geometric coverage models presented in §4.2, plus the traditional single doublet solution for the CNO doublets. The integrated column densities for the doublet solution are larger than the global fits in all cases. In component 2+2a, the doublet solution is 60% greater than the 2-C model for C IV, while in component 4a, it is 45% and 70% greater for C IV and N V, respectively. Comparing the two global fit models, the CNO column densities from model B are greater than the single C model by 0 – 30%, while the H I column density is 50% less.
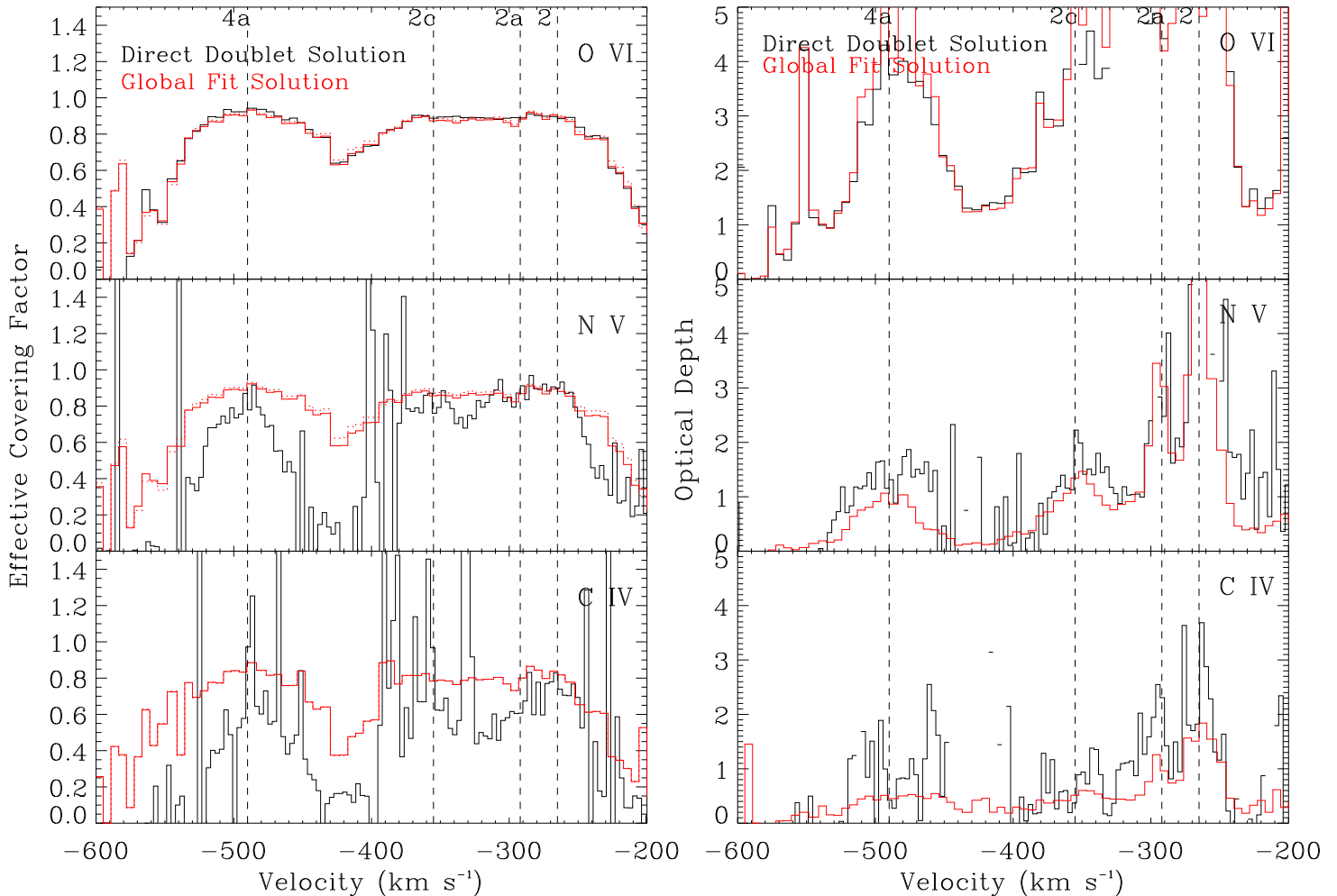
Fig. 9.— Comparison of covering factor and optical depth solutions derived with the global-fit (red) and single doublet (black) methods. Left panels: Covering factors from the global-fitting method are the effective values derived by weighting the individual covering factors in model B by their respective fluxes. The short-wavelength doublet members are plotted with solid red lines and the long-wavelength members with dotted lines. Right panels: Optical depths for the long-wavelength lines of the doublets.

5.3. Constraints on the Nuclear Absorption – Emission Geometry

Here we explore constraints on the nuclear absorption and emission geometry available from the covering factor solutions derived in §4.2. Full analysis of the physical conditions in the outflow, using photoionization modeling of the combined UV and X-ray absorption, will be presented in a future study.

As discussed in §5.1, we adopt the 2-C global fit (model B) for the covering factors and column densities. The covering factor solutions in Figure 5 are consistent with the UV continuum source being fully in our sight-line through the absorber, for all kinematic components, while the emission lines are only partially so. This constrains the relative line-of-sight geometry of the absorbers and nuclear emission sources and places a lower limit on the transverse size of the outflow. Monitoring of time lags between BLR and continuum variations in Mrk 279 by Maoz et al. (1990) gives the size of the BLR, $R_{BLR} = 12$ light days. Thus, the projected size of the

UV absorbers on the plane of the sky, against the AGN emission, is at least $(C^l)^{1/2} \times R_{BLR}$, or ≈ 10 light days in the cores of the absorption components, and possibly decreasing in the wings.

An additional probe of the nuclear geometry is possible because the Lyβ absorption lies on the high-velocity blue wing of the O VI BLR profile, at $v_{BLR} \approx -2200$ km s^{-1}, as discussed in §3.1 and illustrated in Figure 3. Thus, it samples different BLR kinematics than most other absorption lines, which absorb BLR velocities coinciding with the absorption outflow velocities ($v_{BLR} \approx -300$ km s^{-1}). Therefore, comparison of the Lyβ emission-line covering factor and those associated with other lines serves as a probe of the kinematic-spatial structure of the BLR. The potential affect of complex velocity-dependent structure in the BLR on the absorption covering factors was explored in Srianand & Shankaranarayanan (1999). Since we assumed a priori that all lines share the same individual covering factors in the Lyman series fit in §4.2, a legitimate comparison requires obtaining independent constraints on the covering factor of the O VI BLR blue wing by the Lyβ absorber. This comes straightforwardly from the observed Lyγ absorption line, since Lyγ has no underlying line emission. Using the result that $C^c = 1$, the intrinsic optical depth ratio for Lyβ : Lyγ, and the

TABLE 2
INTEGRATED IONIC COLUMN DENSITIES[a]

Ion	Model A: 1 C Fit 2+2a[c]	4a[c]	Model B: 2 C Fit 2+2a	4a	Doublet Method 2+2a	4a	Full Coverage[b] 2+2a	4a
C IV	1.6	0.9	2.1	1.1	3.3	1.6[d]	1.5	0.9
N V	>6.6	2.1	>6.6	2.1	>8.1	3.6	4.7	2.0
O VI	>14	>13	>14	>13	>14	>13	9.8	9.5
H I	7.5	⋯	5.0	⋯	⋯	⋯	4.4[e]	⋯

[a]All column densities in units of 10^{14} cm^{-2}; for doublets, measurements are for the red member; lower limits are quoted for lines with regions having $\tau \geq 3$
[b]$C = 1$ assumed everywhere.
[c]Component 2+2a, $v = -230 - -315$ km s^{-1}; Component 4a, $v = -435 - -535$ km s^{-1}
[d]Integrated over limited range due to infinities in solution.
[e]Using Lyγ line.

observed Lyγ profile, the absorption profile for Lyβ can be derived as a function of C^l from equation 4. Some illustrative results are shown in Figure 10. This shows, for example, that both an unoccluted and fully occulted high velocity O VI BLR are ruled out by the data. We find that values ranging from $0.5 \lesssim C^l \lesssim 0.8$ are required to fit the majority of the Lyβ absorption in components $2 - 2a$. This is similar to the emission line covering factor derived from the global fit to the CNO doublets (Figure 5b). Additionally, the Lyα C^l profile can be derived independently for comparison with Lyβ, in a similar manner as for Lyβ (i.e., using $C^c = 1$, the observed Lyγ profile, and the Lyα : Lyγ τ ratio). The result is identical to the solution to the combined Lyman lines in components $2 - 2a$ shown in Figure 5a within uncertainties. Therefore, the absorption covering factor of the O VI BLR emission at $v_{BLR} \approx -2200$ km s^{-1} is similar to C^l at lower emission-line velocities (by the CNO doublets and Lyα). These results may provide constraints for models of the BLR, e.g., testing disk vs spherical geometries and outflow vs rotational kinematics for the BLR.

6. SUMMARY

We have presented a study of the intrinsic UV absorption in the Seyfert 1 galaxy Mrk 279 from an analysis of combined long observations with *HST*/STIS and *FUSE*. These spectra were obtained simultaneously in May 2003 as part of an intensive multiwavelength observing campaign.

We present a review of the standard technique for measuring intrinsic UV absorption parameters based on individual doublet pairs, showing some key limitations of this method: 1) It cannot treat multiple background emission sources. This introduces a potential error in the solution and misses important geometric constraints on the outflow. 2) Using synthetic absorption profiles, we show it systematically underestimates the covering factor (and overestimates τ) in response to spectral noise. The discrepancy in the solution is shown to be strongly dependent on absorption strength.

To measure the UV absorption parameters in Mrk 279, we independently fit two groups of lines: the Lyman series lines and the combined CNO lithium-like doublets. The doublet fitting involved a global fitting approach, which assumes the same covering factors apply to all ions. By increasing the number of lines that are simultaneously fit, more complex and physically realistic models of the absorption-emission geometry can be explored. Solutions for two different geometrical models, one assuming a single covering factor for all background emission and the other separate covering factors for the continuum and emission lines, both give good statistical fits to the observed absorption. However, several lines of evidence support the model with two covering factors: 1) the independently fit Lyman lines and CNO doublets give similar solutions to the covering factors of both emission sources; 2) the fits are consistent with absorbers that fully occult the continuum source and partially cover the emission lines, consistent with the relative sizes of the emission sources; and 3) observed variability in the Lyα absorption depth can be explained naturally by this model as a change in effective covering factor resulting from a change in the relative strengths of the emission components.

Comparison of the traditional solutions based on individual doublets and the global-fit solutions shows the former exhibits much stronger velocity dependence. This is seen as decreases in covering factor in the wings of individual kinematic components, and as peculiar fluctuations in both τ and C in other regions of relatively weak absorption. In light of the systematic errors shown to be inherent in the individual doublet solution, we conclude some of these effects are likely artifacts of the solution and should be interpreted with caution.

The covering factor solutions from our global fit constrains the relative line-of-sight geometry of the absorbers and nuclear emission sources. The derived emission line covering factor, combined with the size of the BLR, constrains the projected size of the absorber to be $\gtrsim 10$ light days. We utilize the coverage of the high velocity O VI BLR by the Lyβ absorber to explore kinematic structure in the BLR; we find no evidence for dependence of the absorber's BLR covering factor on the BLR velocity.
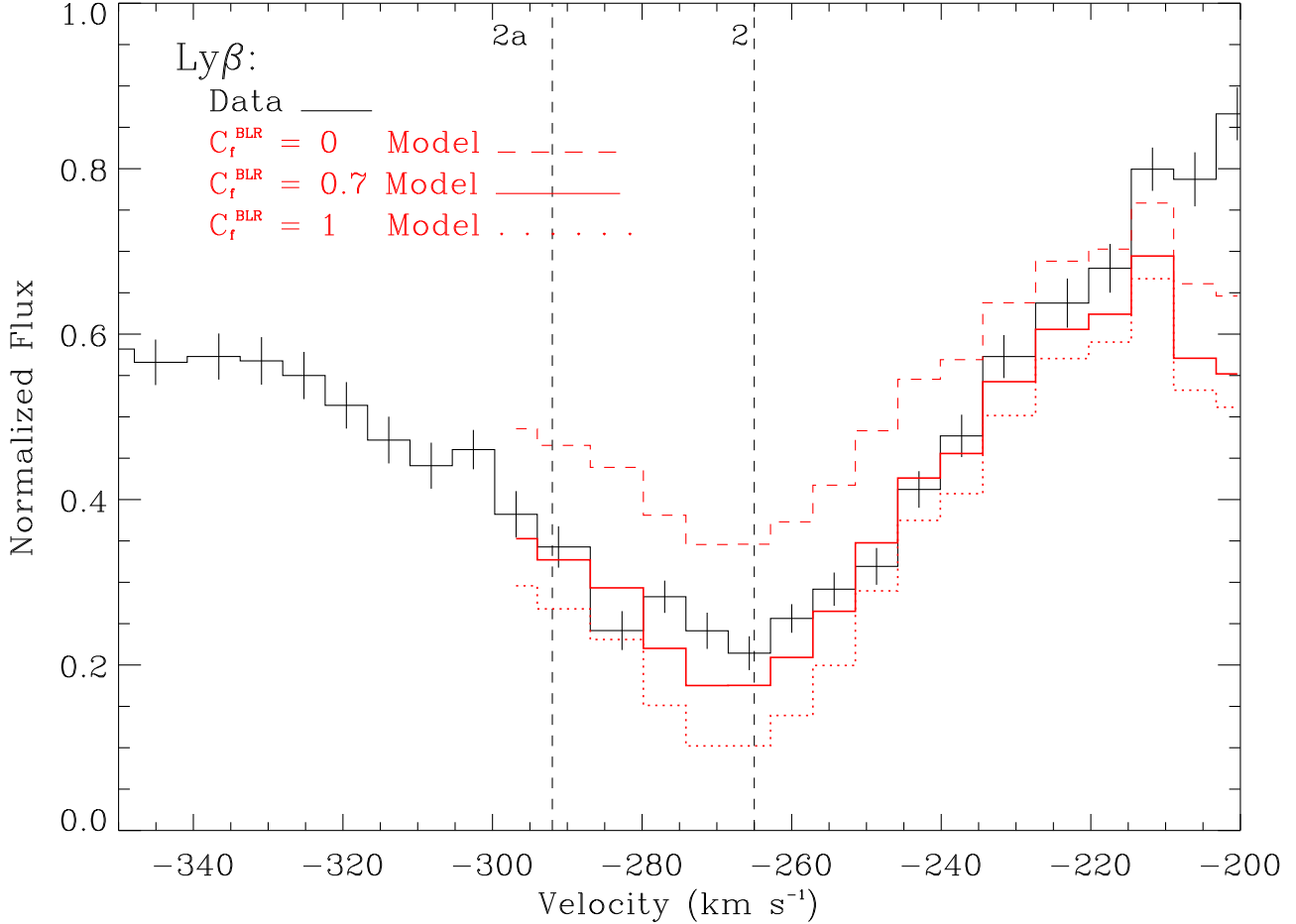
Fig. 10.— Constraints on the covering factor of the high blueshifted velocity O VI BLR by the Lyβ absorber. The observed normalized Lyβ profile (black) is compared with models derived for three values of emission-line covering factor (red). Models were derived using the observed Lyγ absorption, as described in the text. Models with an unocculted (dashed) and fully occulted (dotted) BLR are ruled out. An emission line covering factor of 0.7 (solid), consistent with the global fits, matches most of the observed profile well.

Hall for comments that helped clarify and improve this study.

7. APPENDIX

Here, we address how the expressions for covering factor and optical depth from the doublet solution (equations 2 and 3) depend on noise in the spectrum. We have generated synthetic absorption profiles for doublet pairs that include random fluctuations to simulate spectral noise. We derive the $C - \tau$ solutions for these synthetic profiles to determine any trends in the solution as a function of noise level and absorption strength.

Our synthetic profiles were derived in the following way. The optical depth profiles were assumed to be Gaussian, parameterized by the width (σ) and peak optical depth in the core of the blue line (τ_{max}). The "true" normalized absorption profiles for the lines are then derived from equation 1, with the covering factors set at a constant value across the profile for each doublet pair, and $\tau(v)_r = \tau(v)_b/2$ at all velocities. Thus, we have assumed in effect a single background emission source to avoid the complications described in §3.1. For comparison with our study of Mrk 279, we have set the velocity resolution of our synthetic profiles to that of the STIS

E140M grating, and the absorption width ($\sigma = 50$ km s^{-1}) to be approximately consistent with intrinsic absorption components 2–2c. To simulate spectral noise, we generated a normally distributed random number associated with each velocity bin in the synthetic spectra. The noise level was normalized by selecting the desired S/N in the unabsorbed continuum and then weighting the noise by flux level, S/N$(v) \propto I(v)^{1/2}$, according to Poisson statistics.

We generated profiles for a range of S/N, C (real), and τ_{max}. Here, we give some brief illustrative results, while reserving a full analysis for a later study. The left panels in Figure 11 show synthetic profiles for doublet pairs with $\tau_{max} = 2$, 1, 0.5, and 0.25. In all cases, $C = 0.8$ and the noise level was normalized to be 3% in the continuum. The middle two panels show the corresponding covering factor and optical depth profiles derived directly from equations 2 and 3, with the actual values marked with dashed lines for comparison. Errors in the doublet solution are immediately apparent. The covering factors are systematically underestimated, and the magnitude of error is strongly dependent on absorption strength. This is seen both in the lower covering factors derived in the cores of features with lower τ_{max} (means and stan-

dard deviations measured over the central $150\,\mathrm{km\,s^{-1}}$ are printed in each plot), and in the decrease in C computed in the wings of each profile.

These systematic errors are due to non-linear effects in the doublet equations. This is seen most clearly by comparing the numerator, $N = (I_r - 1)^2$, and denominator, $D = I_b - 2I_r + 1$, in the expression for covering factor (equation 2). The right panels of Figure 11 show the values of D and N/C (in red), which would be identical in each velocity bin for infinite S/N. Due to the forms of N and D, these quantities have very different dependences on noise; $\Delta N/N$ becomes much smaller than $\Delta D/D$ for weak absorption and, at sufficiently small τ, N is less than the noise level of D. As N decreases relative to the noise in D for weaker absorption, the probability that $0 \leq D \leq N/C$ becomes vanishingly small, and the average value of N/D becomes increasingly small.

These errors could have pronounced effects on the interpretation of the outflow. Each solution that underestimates C overestimates τ. Thus, ionic column densities are systematically overestimated, with increasing relative discrepancies in weaker doublets, leading to errors in determining the ionization structure and total gas in the absorber via photoionization models. Additionally, the errors in covering factor solutions will effect geometric inferences. For example, due to the high-ionization state of AGN outflows, lower-ionization species appearing in UV spectra are generally weaker. Thus, the increasing discrepancy in weaker absorption doublets may lead to the misinterpretation of ionic-dependent covering factors. Also, weaker absorption in the wings of an absorption feature could lead to apparent velocity-dependent covering factors that are instead due to optical depth variations, or at least exaggerate the effect.
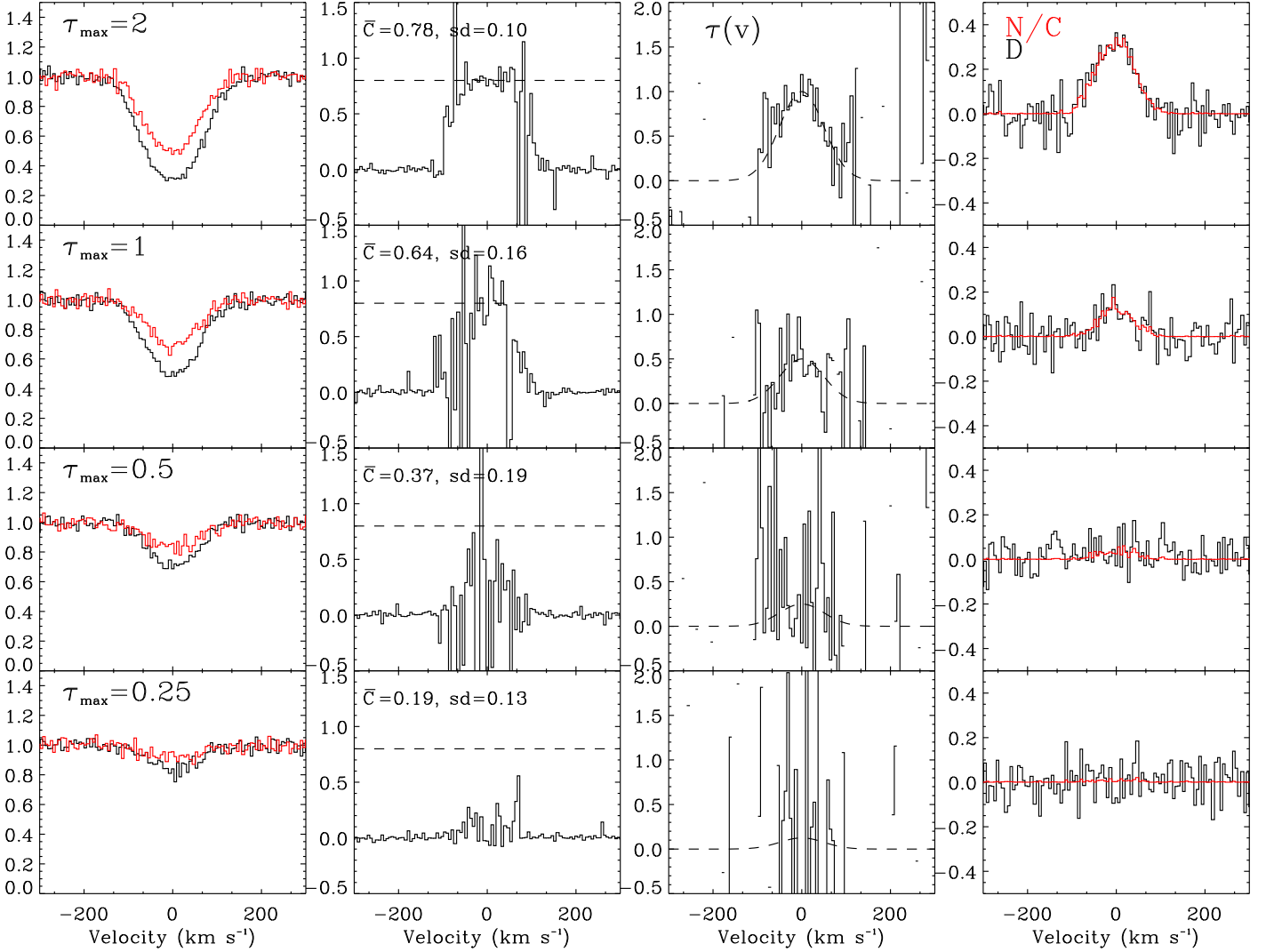
FIG. 11.— Systematic errors in the doublet solution resulting from spectral noise. Left panels show synthetic normalized doublet profiles (long wavelength members in red) with simulated noise for a range of absorption strengths. The peak τ in the blue doublet member is given at the top of each panel. Middle panels show C profiles derived from the doublet solution (equation 3); means and standard deviations (sd) measured in the central 150 km s^{-1} are printed. The actual constant covering factor, $C = 0.8$, is denoted with a dashed line for comparison. Right panels show the value of the numerator (N) of the doublet equation divided by C (red), which would be identical with the denominator (D, black) for infinite S/N. However, due to the non-linear form of N, N/C drops below the noise level in D for low τ. The result is a sytematic underestimation of C, with increasing discrepancy for weaker absorption.

REFERENCES

Arav, N., et al. 2004, ApJ, in press

Arav, N., Korista, K. T., & de Kool, M. 2002, ApJ, 566, 699

Arav, N., Becker, R. H., Laurent-Muehleisen, S. A., Gregg, M. D., White, R. L., Brotherton, M. S., & de Kool, M. 1999, ApJ, 524, 566

Blandford, R, D., & Begelman, M. C. 2004, MNRAS, 349, 68

Blandford, R, D., & Begelman, M. C. 1999, MNRAS, 303, L1

Barlow, T. A., & Sargent, W. L. W. 1997, AJ, 113, 136

Bevington, P. R. 1969, Data Reduction and Error Analysis for the Physical Sciences, pp 242-245

Bohlin, R. C., Dickinson, M. E., & Calzetti, D. 2001, AJ, 122, 2118

Cardelli, J. A., Clayton, G. C., & Mathis, J. S. 1989, ApJ, 345, 245

Cavaliere, A., Lapi, A., & Menci, N., 2002, ApJ, 581, L1

Cohen, M. H., Ogle, P. M., Tran, H. D., Vermeulen, R. C., Miller, J. S., Goodrich, R. W. & Martel, A. R. 1995, ApJ, 448, L77

Costantini, E., et al. 2004, ApJ, in press

Crenshaw, D. M., Kraemer, S. B., & George, I. M. 2003, AARA, 41, 117

Crenshaw, D. M., Kraemer, S. B., Boggess, A., Maran, S. P., Mushotzky, R. F., & Wu, C.-C. 1999, ApJ, 516, 750

de Kool, M., Korista, K. T., & Arav, N. 2002, ApJ, 580, 54

de Kool, M., Arav, N., Becker, R., Laurent-Muehleisen, S. A., White, R. L., Price, T., Gregg, M. D. 2001, ApJ, 548, 609

Gabel, J. R., Kraemer, S. B., & Crenshaw, D. M. 2004, in AGN Physics with the Sloan Digital Sky Survey, eds. G. T. Richards & P. B. Hall (San Francisco: ASP), p239

Gabel, J. R., et al. 2003, ApJ, 583, 178

Ganguly, R., Eracleous, M., Charlton, J. C., & Churchill, C. W. 1999, AJ, 117, 2594

George, I. M., Turner, T. J., Netzer, H., Nandra, K., Mushotzky, R. F., & Yaqoob, T. 1998, ApJS, 114, 73

Goodrich, R. W., & Miller, J. S. 1995, ApJ, 448, L73

Hall, P. B., Hutsemekers, D., Anderson, S. F., Brinkmann, J., Fan, X., Schneider, D. P., York, D. G. 2003, ApJ, 593, 189

Hamann, F., Barlow, T. A., Junkkarinen, V., & Burbidge, E. M. 1997, ApJ, 478, 80

Heap, S. R. & Brown, T. M. 1997, in The 1997 HST Calibration Workshop with a New Generation of Instruments, ed. S. Casertano (Baltimore: STScI), 114

Kaastra, J. S., et al. 2004, ApJ, in press

Kaspi, S., Smith, P. S., Netzer, H., Maoz, D., Jannuzi, B. T., & Giveon, U. 2000, ApJ, 533, 631

Kriss, G. A. 2002, in ASP Conf. Ser. 255, Mass Outflow in Active Galactic Nuclei: New Perspectives, ed. D. M. Crenshaw, S. B. Kraemer, & I. M. George (San Francisco: ASP), 69

Kraemer, S. B., et al. 2001, ApJ, 551, 671

Kraemer, S. B., Crenshaw, D. M., George, I. M., Netzer, H., Turner, T. J., & Gabel, J. R. 2002, ApJ, 577, 98

Laor, A. & Netzer, H. 1989, MNRAS, 238, 897

Lindler, D., & Bowers, C. 2000, BAAS, 197, 1202

Maoz et al. 1990, ApJ, 351, 75

Peterson, B. M., Wanders, I., Bertram, R., Hunley, J. F., Pogge, R. W., Wagner, R. M. 1998, ApJ, 501, 82

Proga, D. 2003, ApJ, 585, 406

Reynolds, C. S. 1997, MNRAS, 286, 513

Scannapieco, E., & Peng Ho, S., 2004, ApJ, submitted, astro-ph/0401087

al. 2004, ApJS, 152, 1 (SK04)

Silk, J., & Rees, M. J., 1998, A&A 331, L1S

Srianand, R., & Shankaranarayanan, S., 1999, ApJ, 518, 672

Wakker, B. P., Kalberla, P. M. W., van Woerden, H., de Boer, K. S., & Putman, M. E. 2001, ApJS, 136, 537

Wampler, E. J., Bergeron, J., & Petitjean, P. 1993, A&A, 273, 15